Experimental study of liquid droplets impact on powder surface: The application of effective dimensionless parameters in analysis

Siqi Li*, *Hourong* Yu, and *Haisheng* Fang

Huazhong University of Science and Technology, School of Energy and Power Engineering, 1037 Luoyu Road, Wuhan, China

Abstract. Spreading dynamics of liquid droplets impacting onto powder bed are experimentally studied using high-speed photography. Dimensionless numbers—We, Re, the modified We^* and Re^* corrected by substrate deformation—are used to analyze the impact behaviors of droplets. The spreading time and the maximum spreading factor are further analyzed. The spreading time is accurately described by a universal scaling law that is obtained from the modified dimensionless time vs. the effective Weber number (We^*), and the maximum spreading factor is found to follow the modified classic scaling law $\beta_{\max} = f(We^*, Re^*)$.
Keywords: Maximum spreading, Effective Weber number, Spreading time, Droplet impact.

1 Introduction

Droplet impact on powder beds occurs extensively in industrial and technological applications, such as granulation in the pharmaceutical industry[1,2]; granule formation by spraying for powder coating and spray drying[3,4]; and in three-dimensional printing processes[5–7]. It is important to understand the dynamics of the droplet impact process on powder beds, which is critical for controlling such processes. Various impact behaviors—e.g., spreading, retraction, rebounding, and splashing—and the resulting crater morphology as well as, liquid marbles have been investigated in detail[8–10] . The behaviors of droplets upon impact have been studied comprehensively by experimental[11,12], theoretical[13,14], and numerical methods[15].

In the experimental and theoretical study, the impact dynamics of liquid droplets and powder surfaces have been systematically investigated. The influences of initial impact velocity and liquid properties on spreading time and maximum spreading have been examined. By using modified Weber number and Reynolds number, we apply empirical expressions for non-deformable solid substrate to powder bed, and reveal their similarities for maximum spreading and spreading time. Scaling analyses were adopted to reveal three characteristic parameters.

* Corresponding author: m201971069@hust.edu.cn

2 Experimental setup and mathematical models

Alumina beads were supplied by the manufacturer Hebei Xinda Alloy material, China. The initial packing fraction, Φ, was reproducible for successive repeat experiments. And in the experiments, Φ is controlled in the range of 0.58 - 0.60 by using tight compression.

Liquids and their properties used in the experiments are displayed in **Table** 1. Dimensionless parameters used in the analysis are Weber number We, and the Reynolds number Re: $We = \rho D u_i^2/\sigma$; $Re = \rho u_i D/\mu$; where ρ, μ, D, and σ are, respectively, liquid density, liquid dynamic viscosity, droplet impact diameter, and liquid surface tension factor; g is the gravitational acceleration and $u_i = \sqrt{2g(h_r - D)}$ is the velocity at the time of impact. The droplet is released onto powder bed from different heights ranging from 3 to 600 mm, resulting in impact velocity range from 0.2 to 3.2 m/s. Droplets can be considered as sphere upon impact. The equilibrium contact angle, θ, is also measured.

The experimental setup (**Fig**. **1**) includes a high-speed video camera (Qianyanlang 5KF20), which can capture the impact, spreading, and penetration in a single video sequence.

Table 1. Physical properties of liquids used.

Liquid	D (mm)	ρ (kg·m^{-3})	μ (mPa·s)	σ (N·m^{-1})	θ(°)
Water	2.10	997	1.003	0.072	86.60
50%ethanol	1.78	900	1.10	0.0279	61.66
Ethanol	1.89	789	1.19	0.0232	66.9
50%glycerinum	2.27	1120	4.21	0.070	57.62
Glycerinum	2.26	1260	1410	0.063	37.70
20% glycol	2.42	1029	1.65	0.0605	66.00
50% glycol	2.41	1073	3.94	0.056	63.87
80% glycol	2.18	1110	10.05	0.0504	68.31
Glycol	2.17	1113	21.00	0.0484	58.23
Acetone	1.66	791	0.306	0.0237	72.77

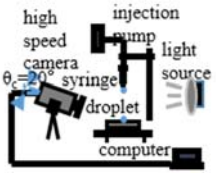

Fig. 1. Schematic of the experimental setup used.

3 Results and discussion

3.1 Spreading time t_s

Fig. 2(a) depicts the spreading time t_s as a function of the impact velocity. The spreading time is typically a few milliseconds, which is of the same order of magnitude as the characteristic advective time[16] $\tau_a = d_0/(2u_i)$ or the capillary-inertial time[17] $\tau_i = (\rho d_0^3/8\sigma)^{0.5}$. **Fig. 2**(b) shows that t_s decreases sharply as the impact velocity increases for $We^* \leq 40$ but slowly decreases for $We^* > 40$. Since τ_a and τ_i ignore influences such as viscosity and surface wettability, a modified capillary-inertia time $\tau_{i'} = (\rho d_{max}^3/8\sigma)^{0.5}$ is adopted to study the spreading[18], where d_{max} is related to liquid viscosity and wettability. **Fig. 2**(c) shows a log-log plot of normalized spreading time $t_s/\tau_{i'}$ vs. We^*. This shows that the function $t_s/\tau_{i'} = \zeta We^{*\lambda}$ gives a good fit to the experimental data. The fitting coefficient ζ and the exponent λ for different viscosities are shown in **Fig. 2**(d). The quantities ζ and λ appear to be independent of liquid viscosity and substrate wettability. Consequently, a universal empirical expression, $t_s/(\rho d_{max}^3/8\sigma)^{0.5} = 1.46 We^{*-0.46}$, can accurately describe the spreading time in powder bed experiments.

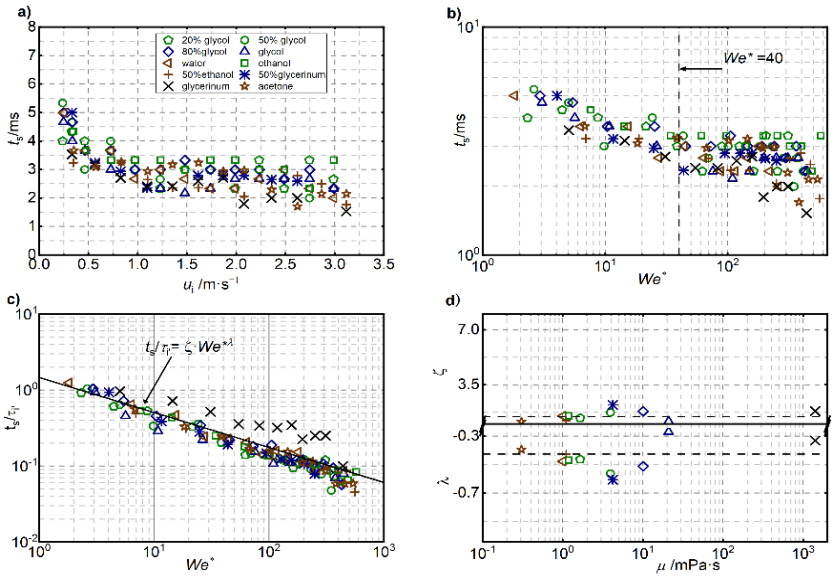

Fig. 2. (a) Spreading time $t_s$vs. impact speed u_i. (b) Spreading time t_s vs. effective Weber number We^*. (c) Normalized spreading time t_s/τ_i, vs. We^*. (d) The coefficient ζ and exponent λ of the graph in part (c) vs. liquid viscosity.

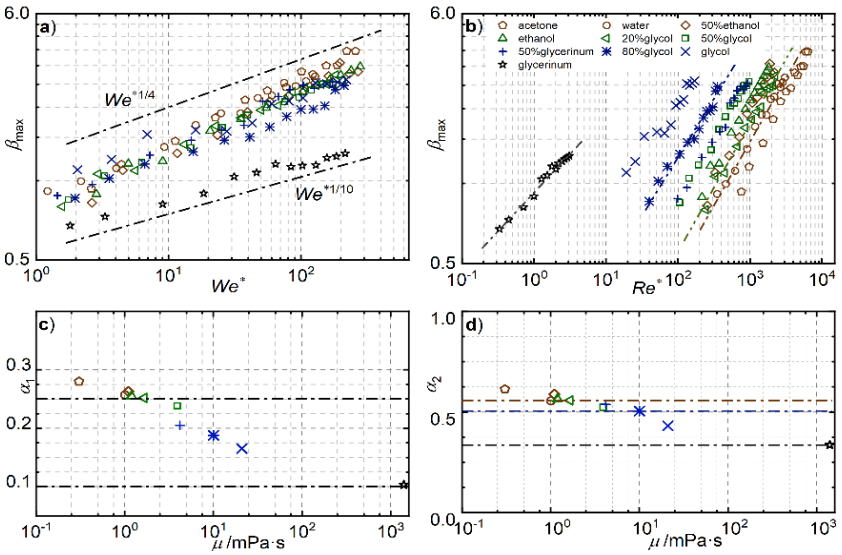

Fig. 3. The maximum spreading factor β_{max} vs (a) We^* and (b) Re^* for all liquids. The maximum spreading factors were fitted in (a) with $\beta_{max} = A_1 We^{*\alpha 1}$and in (b) with $\beta_{max} = A_2 Re^{*\alpha 2}$. α_1 and α_2 as functions of liquid viscosity are plotted in (c) and (d).

3.2 Maximum spreading factor β_{max}

An effective Weber number $We^* = [D/(D + 2Z_m)]We$, where Z_m is the maximum vertical deformation measured[11], is used to replace *We*. It has been shown that We^* collapses the maximum spreading data for various packing densities[19], indicating that We^* can also characterize the effect between liquid droplets with various viscosity and the powder bed

with the same packing fraction. **Fig. 3** gives the correlation of $\beta_{\max}$ vs We^* ($We^* = [D/(D + 2Z_m)]We = We^I$) and the correlation of $\beta_{\max}$ vs Re^* ($Re^* = [D/(D + 2Z_m)]Re \neq Re^I$, because the value of $\frac{Re}{Re^I} = \frac{\rho v_p}{\mu} = \frac{2(1-\phi)^4 d_g^2 \left[\frac{2\sqrt{6}(D+2Z_m)\sigma^{0.5}\rho^{1.5}u_i D^{-1.5}}{\sqrt{\pi}} + \frac{4\rho\sigma\cos\theta}{d}\right]}{[\mu^2(180\phi^2)]}$ depends heavily on viscosity, Re^I is not applicable to the analysis of viscosity effect in this paper, **Fig. 4** also proves this point) respectively for various viscosity liquids. As shown in **Fig. 3** (a) and (c), a scaling law behavior, $\beta_{max} \sim We^{*\alpha 1}$, is observed at $We^* > 1$. It comes as no surprise to see that $\beta_{\max}$ increases with We^*. The data set exhibits three other distinguished features: (1) The maximum spreading factor is suppressed with increasing viscosities (different color symbols in **Fig. 3** (a)). (2) In the doubly logarithmic scale, there are two asymptotes in the extension of data: the upper is $We^{*1/4}$ and the lower is $We^{*1/10}$. (3) The value of α_1 decreases with increasing viscosities (**Fig. 3**(c)). On the other hand, it seems that the spreading is dominated by viscous force within the liquid for all experimental data. In **Fig. 3**(b), $\beta_{\max}$ grows with Re^* following the power law, $\beta_{\max} \sim Re^{*\alpha 2}$.The exponent α_2 is ~0.5 for lowly viscous liquids with $\mu \leq 10$ mPa·s, and it decreases to ~0.33 for liquids with $\mu = 1430$ mPa·s.

Because of the quantitative relation $We^{1/10} \sim D^{-1/4}Re^{1/5}$, a law of the type $\beta_{\max} \sim We^{*1/10}$ leads to $\beta_{\max} \sim Re^{1/5}$. According to the analysis of the transition to a viscous regime, we thus define the effective number $P^* \equiv We^*/Re^{*4/5}$ for deformable substrate ($P \equiv We/Re^{4/5}$ for non-deformable substrate[20]). The transition between the capillary regime and viscous regime is plotted in **Fig. 4**(a), where the dimensionless viscous extension $\beta_{max}/Re^{*1/5}$ is plotted as a function of P^*. While for $P^\dagger = We^\dagger/Re^{\dagger 4/5}$ in **Fig. 4**(b), the result is surprisingly that the transition is opposite to **Fig. 4**(a)—the viscous droplet spreading changes from viscous regime to the capillary regime as $P^\dagger$ increases. Consequently, $Re^\dagger$ — incorporates the bulk wettability of a granular substrate—doesn't fit to interpret the influence of liquid viscosity on spreading. The use of We^* and Re^* reveals the hidden similarities between a droplet impact on deformable substrate and that on a non-deformable substrate for maximum droplet spreading. Same as the non-deformable substrate, the influence of internal inertial flow at maximum spreading phase also exists, and causes the maximum spreading smaller than the theoretical value.

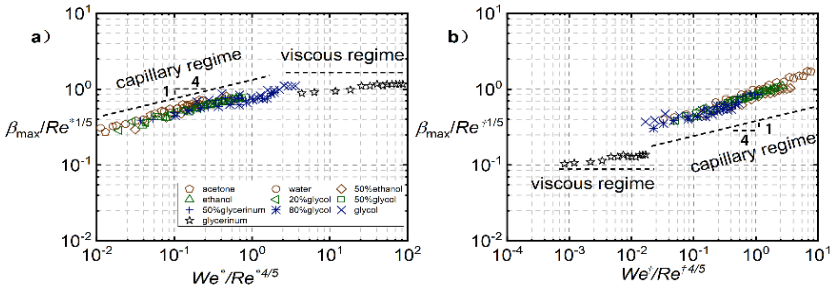

Fig. 4. (a) The maximum spreading factor $\beta_{\max}$ of **Fig. 3** in a doubly logarithmic plot. (b) is based on (a), but $We^*$and Re^* are replaced by $We^\dagger$ and $Re^\dagger$.

4 Conclusions

We have performed an experimental study of various liquid droplets impacting alumina powder beds. Weber numbers (We) and Reynolds numbers (Re) were obtained by adjusted the droplet fall height. Ten liquids were used that provided various viscosities and various surface tensions.

Then we adopted spreading time t_s and maximum spreading factor $\beta_{\max}$ to quantitatively analyze the spreading behavior of the droplets after impacting the powder bed. The modified

capillary-inertial time $\tau_{i'} = (\rho d_{max}^3/8\sigma)^{0.5}$considering the influence of substrate wettability and liquid viscosity, and the effective Weber number $We^* = [D/(D + 2Z_m)]We$ considering the influence of the deformable substrate, are innovatively put forward to achieve a universal scaling law: $t_s/(\rho d_{max}^3/8\sigma)^{0.5} = 1.46We^{*-0.46}$. Besides, the effective weber number We^*, replacing traditional weber number, is adopted to attain the scaling law $\beta_{max} \sim We^{*\alpha 1}$, and α_1 decreases with the increasing viscosity. The same thing happens for the scaling law $\beta_{max} \sim Re^{*\alpha 2}$. The capillary regime considered implies a small P^* ($P^* = We^*/Re^{*4/5} < 1$), the viscous regime refers to large P^* ($P^* = We^*/Re^{*4/5} > 10$). Thus, the use of We^* and Re^* reveals the hidden similarities between a droplet impact on deformable substrate and that on a non-deformable substrate for maximum droplet spreading.

This study is supported by Grants from National Natural Science Foundation of China (No. 51876071).

References

1. Hapgood, K. P. & Khanmohammadi, B. Powder Technol. **189**, 253–262 (2009).
2. Knight, P. C. Powder Technol. **119**, 14–25 (2001).
3. Kayrak-Talay, H. N. E. and D. J. D. L. IFAC Proc. Vol. (2012) doi:10.1002/aic.
4. Moreira, A. L. N., Moita, A. S. & Panão, M. R. Prog. Energy Combust. Sci. **36**, 554–580 (2010).
5. Sachs, E., Cima, M., Williams, P., Brancazio, D. & Cornie, J. J. Manuf. Sci. Eng. Trans. ASME **114**, 481–488 (1992).
6. van Dam, D. B. & Le Clerc, C. Phys. Fluids **16**, 3403–3414 (2004).
7. Van Der Bos, A. *et al.* Phys. Rev. Appl. **1**, 1–9 (2014).
8. Rioboo, R., Marengo, M. & Tropea, C. Exp. Fluids **33**, 112–124 (2002).
9. van der Meer, D. Annu. Rev. Fluid Mech. **49**, 463–484 (2017).
10. Delon, G., Terwagne, D., Dorbolo, S., Vandewalle, N. & Caps, H. Phys. Rev. E - Stat. Nonlinear, Soft Matter Phys. **84**, 3–7 (2011).
11. De Jong, R., Zhao, S. C., Garcia-Gonzalez, D., Verduijn, G. & Van Der Meer, D. Soft Matter **17**, 120–125 (2021).
12. Hardt, S. & McHale, G. Annu. Rev. Fluid Mech. **54**, 83–104 (2022).
13. Li, S. *et al. Science Advances* vol. 7 (2021).
14. Graeber, G. *et al.* Nat. Commun. **12**, 1–7 (2021).
15. Yarin, A. L. Annu. Rev. Fluid Mech. **38**, 159–192 (2006).
16. Supakar, T., Moradiafrapoli, M., Christopher, G. F. & Marston, J. O. J. Colloid Interface Sci. **468**, 10–20 (2016).
17. Wildeman, S., Visser, C. W., Sun, C. & Lohse, D. J. Fluid Mech. **805**, (2016).
18. Lin, S. *et al.* J. Colloid Interface Sci. **516**, 86–97 (2018).
19. Zhao, S. C., De Jong, R. & Van Der Meer, D. Soft Matter **11**, 6562–6568 (2015).
20. Clarke, A., Blake, T. D., Carruthers, K. & Woodward, A. Langmuir **18**, 2980–2984 (2002).